An Evaluation of Two-Photon Excitation Versus Confocal and Digital Deconvolution Fluorescence Microscopy Imaging in Xenopus Morphogenesis

AMMASI PERIASAMY,[1,2]* PAUL SKOGLUND,[2] COLTEN NOAKES,[1,2] AND RAYMOND KELLER[2]
[1]*W.M. Keck Center for Cellular Imaging, Gilmer Hall, University of Virginia, Charlottesville, Virginia 22903*
[2]*Department of Biology, Gilmer Hall, University of Virginia, Charlottesville, Virginia 22903*

KEY WORDS two-photon excitation; confocal; digital deconvolution; point spread function; fluorescence microscopy; deep tissue imaging; green fluorescent protein; xenopus morphogenesis; embryos

ABSTRACT The ability to visualize cell motility occurring deep in the context of opaque tissues will allow many currently intractable issues in developmental biology and organogenesis to be addressed. In this study, we compare two-photon excitation with laser scanning confocal and conventional digital deconvolution fluorescence microscopy, using the same optical configuration, for their ability to resolve cell shape deep in Xenopus gastrula and neurula tissues. The two-photon microscope offers better depth penetration and less autofluorescence compared to confocal and conventional deconvolution imaging. Both two-photon excitation and confocal microscopy also provide improved rejection of "out-of-focus" noise and better lateral and axial resolution than conventional digital deconvolution microscopy. Deep Xenopus cells are best resolved by applying the digital deconvolution method on the two-photon images. We have also found that the two-photon has better depth penetration without any degradation in the image quality of interior sections compared to the other two techniques. Also, we have demonstrated that the quality of the image changes at different depths for various excitation powers. *Microsc. Res. Tech. 47:172–181, 1999.*

INTRODUCTION

Fluorescence microscopy has become one of the commonly used techniques to visualize structural information of living specimens. Furthermore, the technology development and new fluorescent probes such as green fluorescent proteins have revolutionized light microscopy imaging in living biological samples (Bright and Taylor, 1986; Chalfie et al., 1994; Inoué and Spring, 1997; Periasamy and Herman, 1994; Sullivan and Kay, 1999; Tsien, 1989). The wide-field digital deconvolution and the laser scanning confocal helped biologists to improve the image quality of the cells from fixed and live specimens. But there was always a struggle in deep tissue imaging and handling the UV fluorophore for cellular imaging, which was solved after the invention of two-photon excitation microscopy system (Denk et al., 1990). There are comparisons between confocal and two-photon excitation techniques (Hell et al., 1994; Potter, 1996) but to our knowledge such a comparison for three systems to visualize the live thick biological specimen is not available.

A major problem in visualizing the structures of thick tissue has been the contribution of a signal from above and below the plane of focus, which produces a background glow and results in degradation of the image. To remedy these problems and produce more reliable three-dimensional data, the most widely used techniques are digital deconvolution and confocal microscopy (Chen et al., 1995; Diaspro et al., 1996; Shaw, 1993; White et al., 1987). A confocal microscope uses a pinhole aperture to restrict the "out-of-focus" flare reaching a single detector, the photomultiplier tube (PMT). Because of the pinhole aperture, the entire fluorescence signal collected by the objective lens is not used (Pawley, 1995; Shotton, 1989; Wilson and Sheppard, 1984). In order to increase the signal, increased excitation laser intensity is used, but this will often introduce photobleaching and photodamage. Unlike the confocal configuration, digital deconvolution microscopy uses the entire fluorescence signal collected by the objective lens, without the use of pinhole or UV optics, to deliver the emitted light to two-dimensional high-sensitivity and linear CCD detectors. The "out-of-focus" flare introduced into the image at different optical sections is reversed by computer deconvolution through the use of a point spread function (PSF) of the imaging system (Agard et al., 1989).

In contrast, the two-photon excitation has a potential advantage over conventional widefield digital deconvolution (DDM) or laser scanning confocal microscopy (LSCM) because of its intrinsic three-dimensional resolution and the absence of background fluorescence. In two-photon excitation imaging, the photobleaching and autofluorescence are considerably reduced since the infrared pulsed laser light illumination occurs only at

Contract grant sponsor: National Science Foundation; Contract grant number: DBI-9604709; Contract grant sponsor: National Institutes of Health; Contract grant numbers: S10-RR13714, HD-36426; Contract grant sponsor: W.M. Keck Foundation; Contract grant sponsor: Academic Enhancement Program of the University of Virginia.

*Correspondence to: Dr. Ammasi Periasamy, W.M. Keck Center for Cellular Imaging, Gilmer Hall, Department of Biology, University of Virginia, Charlottesville, VA 22903. E-mail: ap3t@virginia.edu

Received 30 July 1999; accepted in revised form 2 August 1999

the focal plane (Denk et al., 1990; Goppert-Mayer, 1931; Hell et al., 1996; Konig et al., 1996; Lakowicz, 1997; Periasamy, 1999; Piston et al., 1994; Potter et al., 1996; So et al., 1995; Wokosin et al., 1996). In DDM and LSCM, however, one-photon UV or visible light illuminates the specimen throughout the whole field of view and a considerable amount of photobleaching occurs above and below the focal plane. Two-photon excitation microscopy (TPEM) is an essential imaging system for thick tissue (deeper) cellular imaging and UV absorption fluorophores.

Amphibian systems have been used to study the process of generating a vertebrate body axis for most of this century. This process entwines sequential cascades of inductive cell fate decisions with morphogenesis (Spemann, 1938). The patterned cellular behaviors driving morphogenesis at gastrulation in the frog *Xenopus laevis* are thought to be identified (Domingo and Keller, 1995; Shih and Keller, 1992a,b), and currently represent the highest resolution cellular description of morphogenesis of early development in any vertebrate. However, the cells comprising Xenopus embryos are not transparent unless fixed and cleared so that it allows only a snapshot image of cells, which were undergoing the dynamic process of morphogenesis. For this reason, dynamic descriptions of cell behaviors based on standard conventional microscopy in living frog tissue undergoing morphogenesis reflects what is occurring on the surface of the embryo or explant, rather than a full three-dimensional image including the baso-lateral aspects of surface cell behavior, or cells in deeper tissue layers. A reliable technique for visualizing the three-dimensional motility of living Xenopus cells in whole embryos or explants undergoing morphogenesis would not only allow confirmation of the spatially and temporally patterned behavior thought to drive gastrulation, but would also significantly facilitate studies designed to elucidate the molecular basis for these behaviors.

A GFP-GAP-43 fusion protein is expressed in developing Xenopus embryos by means of RNA injection of the corresponding in vitro transcribed mRNA. This fusion protein localizes the GFP fluorophore to cell membranes by means of a palmitoylation signal, revealing cell outlines under fluorescence microscopy to provide a convenient marker of cell shape. In this paper, we evaluate three methods for visualizing living cell shapes deep in tissues: two-photon, confocal, and deconvolution microscopy. The usefulness of applying these imaging technologies and labelling techniques to the study of Xenopus morphogenesis will be discussed.

MATERIALS AND METHODS

Specimen Preparation

Embryos. Albino Xenopus embryos were generated by induction of egg laying and in vitro fertilization (Kintner and Melton, 1987) and staged (Nieuwkoop and Faber, 1967) by conventional techniques. Either animal caps were cut as described (Kintner and Dodd, 1991) at stage 8 or intact embryos were mounted between coverglass in 100-mm culture dish chambers in which a hole had been cut in the floor and replaced with coverglass held in place with vacuum grease. These living tissues were cultured in DFA (Keller, 1991) until at least control stage 12 before fluorescence microscopy was performed.

RNA and Injections. Capped in vitro transcribed RNA was prepared using the mMessage mMachine kit (Ambion). Plasmid encoding GAP-43-GFP was linearized with Not I and transcribed with SP6 (Kim et al., 1998). This fusion protein, produced in the lab of Paul Garrity, combines a palymitoylation signal from GAP-43 with Green Fluorescent Protein (GFP) (Chalfie et al., 1994), localizing GFP to the cell membrane. Embryos were injected with 5–20 pg RNA in 3–4 separate injections in the animal half of the embryo for animal caps and in various locations for intact embryo experiments, including vegetal injections. Injections were by standard methods (Kintner, 1988). Briefly, needles pulled (Pul-1, WP Instruments Inc.) from 0.75-mm I.D. glass capillaries (Harvard Apparatus) are mounted on a pressure injection system (Medical Systems Corp.) and in vitro synthesized RNA is front loaded into the needle. Drop sizes are calibrated by means of a normalized reticule, and embryos are injected in 1 $\times$ MBS, 5% Ficoll, and transferred to 1/3 $\times$ MBS after a minimum of 2 hours. MBS is 88 mM NaCl, 0.82 mM $MgSO_4$, 2.4 mM $NaHCO_3$, 1.0 mM KCl, 0.33 mM $Ca(N)_3)_2$, 0.41 mM $CaCl_2$, 10 mM HepespH7.4.

Instrumentation

A schematic diagram of the DDM and LSCM system is shown in Figure 1. The system consists of a Nikon PCM200 confocal microscope based on a galvanometer point-scanning scan head was coupled to a side port of the Nikon TE 200 inverted microscope equipped with epi-fluorescence and transmitted illumination optics (Nikon Inc., Melville, NY). The epi-fluorescent light source was a 100 W Hg arc lamp and a halogen lamp for transillumination with a long working distance condenser (0.52). A Plan Fluor 20X, NA 0.78 multiimmersion (water and oil) objective lens was used for the image acquisition both for the DDM and LSCM image acquisition mode. The Ludl (Ludl Electronic Products Ltd., Hawthrone, NY) neutral density (ND), excitation and emission filter wheels were interfaced to the personal computer through a controller (as shown in Fig. 1) and were driven by the C-Imaging (Compix, Inc., Cranberry Township, PA) software. This software operates both the PCM2000 and DDM data acquisition system. The DDM and LSCM use an arc lamp and lasers (argon-ion, 488 nm; HeNe, 543 nm) as light sources, respectively. An Orca-1 CCD camera (Hamamatsu Photonics System, Middlesex, NY) was installed in another port of the TE200 microscope for DDM. The quantum efficiency in the blue/green spectral region of the Orca-1 is about 50%. The data from the same region of the specimen for LSCM and DDM were acquired on the same optical platform as shown in Figure 1. All images were acquired using filters from Chroma Technology (Brattleboro, VT).

The TPEM image acquisition was implemented in the Nikon TE300 epifluorescent microscope with the same objective lens used for LSCM and DDM in TE200. A built-in lens and the dichroic in the filter cube were used to couple the TE300 externally (no physical connection of microscope and the confocal scan head) to the confocal laser head. The distance between MRC600 and the microscope was adjusted to satisfy the far-focality of the imaging system. It is always advantageous to use a

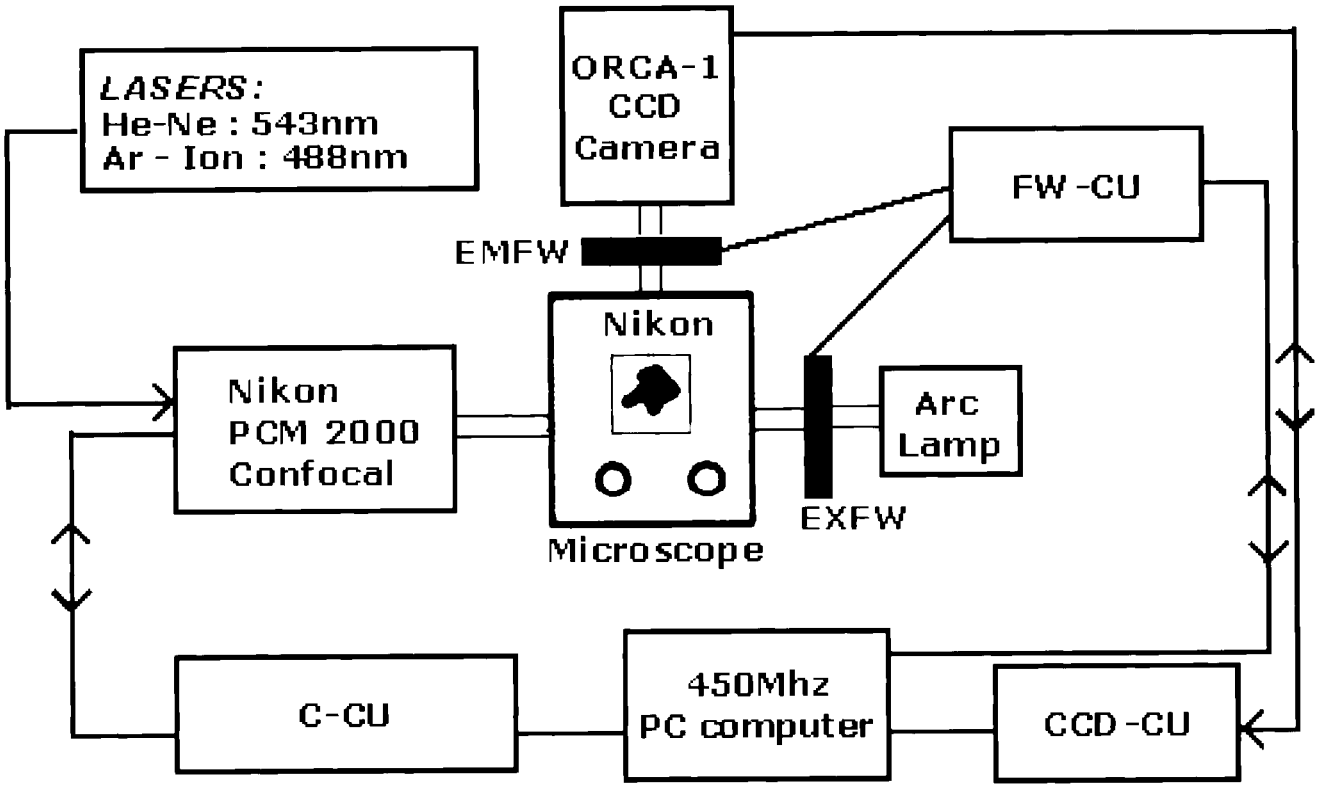

Fig. 1. Schematic illustration of LSCM and DDM. EMFW, emission filter wheel; FW-CU, filter wheel controller; EXFW, excitation filter wheel; CCD-CU, CCD camera control unit; C-CU, confocal control unit.

non-phase objective lens for a laser-based illumination system to minimize any light scattering.

A 5W Verdi pumped, tunable (model 900 Mira) modelocked ultrafast (76 MHz) laser was coupled to the laser port of a Biorad MRC600 (Bio-Rad, Hercules, CA) laser scanning confocal scan head through beam steering optics (Periasamy, 1999). This laser is equipped with x-wave optics for easy tunable range of entire wavelength (700 to 1,000 nm). It is our experience that in order to maintain the stability of the laser power and pulse width, it is important to maintain the same temperature for the room and the baseplate of the Verdi control unit. The silver-coated mirrors for maximum reflections of IR and visible spectrum (Chroma Technology Corp.) replaced the MRC600 conventional mirrors M1, X- and Y-galvo and concave (1 and 2) mirrors. The controller card of the MRC600 and the DOS based software COMOS 7.0a were installed in a 450 MHz Pentium operating Windows '98.

Point Spread Function (PSF)

In imaging, an equivalent blurred point in the image plane replaces every point of the object and the final image is then the sum of all these blurred points. The image would then be the sum of the images of each point constituting the object, i.e., a convolution. The PSF is simply the image of a single point and describes the way the blurring of an individual point occurred in the image plane, or in simple terms, PSF describes the blurring of an image introduced by the microscope optics. The rigorous mathematical derivations can be found in the literature (Chen et al., 1995). A well-measured PSF is key to successful deconvolution or measure of an optical system. Most of the objective lenses are not designed for imaging deep into biological tissue but rather are designed to image objects immediately adjacent to the underside of a cover glass of an exactly defined thickness. Therefore, one should select a good objective lens with high NA for optical sectioning of the specimen. The water immersion lens could be used for imaging deep inside the tissue compared to the oil immersion lens (Periasamy, 1998).

The PSF was measured for DDM, LSCM, and TPEM microscope using sub-microscopic fluorescent beads (i.e., $\leq$0.1 μm). The images of the beads will be good approximations to the PSF, provided the diameters of the beads are well below the resolution limit of the microscope. A suspension of 0.1–3.0 μm beads in glycerol was fixed to the surface of a slide or coverglass, and then a focal series of images of a single bead was recorded in exactly the same way as for a standard biological specimen. The PSF images were acquired with 20× water immersion objective lens (ex = 535/20 nm, dm = 575 nm, and em = 590/35 nm) for LSCM and DDM mode. An excitation wavelength of 780 nm was tuned from a ti:sapphire laser and a 650 SP emission filter was used for acquiring two-photon PSF images. These images were then three-dimensionally reconstructed using the Deltavision (Applied Precision, Mercer Island, WA) software as shown in Figure 2.

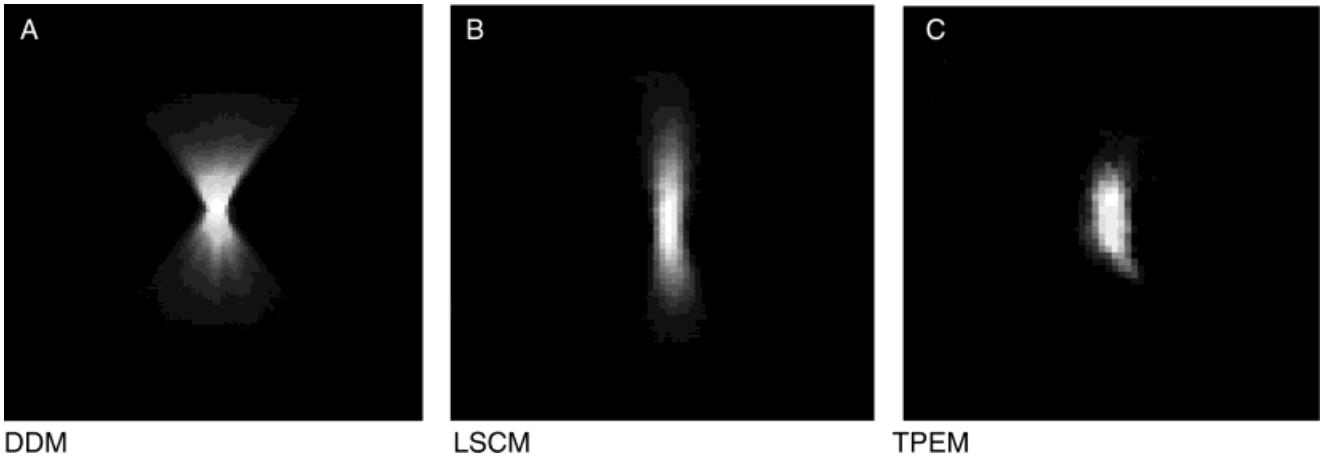

Fig. 2. Three-dimensional reconstruction of point spread function (PSF) of one-micron bead (20X water immersion Plan Fluor objective lens NA 0.78) for DDM, LSCM, and TPEM. The PSF of DDM provides a conventional distribution of point source of light image of a wide-field microscopy. In LSCM and TPEM, the PSF is in elliptical shape. The comparison of LSCM and TPEM clearly reflects the light distribution in the z-plane.

Digital Deconvolution Microscopy (DDM)

Deconvolution is the procedure that reverses the image degradation due to convolution (i.e., inverse Fourier transforms). By modeling the microscope optics as a linear and shift-invariant system, the PSF can be used to describe the transformation of any image by the microscope. A typical fluorescence microscope image can be given by [measured image] = [PSF] * [desired image] where "*" symbol represents the mathematical operation of convolution. The deconvolution ($^{*-1}$), the mathematical inverse of convolution, can be represented as [desired image] = [measured image] ($^{*-1}$) [PSF]. The goal of deconvolution is to solve the equation for the desired image.

Deconvolution improves the resolution of the image acquired at different focal planes to localize or visualize the proteins or molecular structure of the biological specimen in three-dimension (Chen et al., 1995; Periasamy, 1998). Different types of algorithms are used to remove the "out-of-focus" information (Chen et al., 1995). Deconvolution microscopy systems are commercially available and are cheaper than most confocal or two-photon systems. The two-step (optical sectioning and processing later) digital confocal microscope is also referred to as computational optical sectioning, exhaustive photon reassignment, and wide-field deconvolution microscope. Deconvolution requires very intensive computer operation to process the images in a various computer platform (PC, Macintosh, or SGI) in a reasonable amount of time. The interpretation of these images requires some knowledge of the processing methods such that a user can recognize artifacts and identify real features. The disadvantage of this technique is that it is time-consuming, and a two-step process is required to obtain the information of the cellular structure. The DDM system is good for tissue culture cellular imaging but not for deep tissue imaging or monitoring the real-time cell signaling, such as Ca^{2+}.

Laser Scanning Confocal Microscopy (LSCM)

Introduced in 1957, confocal microscopy has gained wide acceptance as an important technology because it can produce images from individual focal planes (Minsky, 1957) in real time. Confocal microscopy removes most of the "out-of-focus" information (blur), by using a pinhole aperture in the emission path (see Fig. 3). This significantly improves lateral resolution and the capacity for direct, non-invasive serial optical sectioning of intact, thick living specimens (Nakumura, 1993; Pawley, 1995; Van der Voort and Brakenhoff, 1988; Wilson and Sheppard, 1984). In confocal microscopy, proper selection of excitation light intensity, sensitivity of the photomultiplier tube, pinhole size, and the concentration of the probe in the specimen give a signal-to-noise (S/N) ratio superior to conventional microscopy. LSCM is widely used for real-time signaling. The excitation light illuminates the entire specimen, thus introducing background emission into the plane of focus and increasing the photobleaching and photodamage to the cell. The photodamage of UV light illumination is a major problem in LSCM.

Two-Photon Excitation Microscopy (TPEM)

In contrast to DDM and LSCM, with two-photon excitation only a diffraction-limited spot is illuminated in the specimen, thereby reducing photobleaching and photodamage outside this limited area (Denk et al., 1990; Goppert-Mayer, 1931; Hell et al., 1996; Periasamy, 1999). Two-photon (2p) excitation occurs when two photons of $h\omega$ and $h\omega'$ are simultaneously absorbed and a molecule is excited to the state of energy $E_e = h\omega + h\omega'$. The probability of two-photon absorption depends on the co-localization of two photons within the absorption cross-section of the fluorophore, and the rate of excitation is proportional to the square of the instantaneous intensity. Two-photon excitation is made possible by the very high local instantaneous intensity provided by a combination of diffraction-limited focusing of a single laser beam in the specimen plane and the temporal concentration of a femtosecond (fsec) mode-locked laser.

The IR light replaces the one-photon UV and visible light excitation. The infrared excitation light has lower

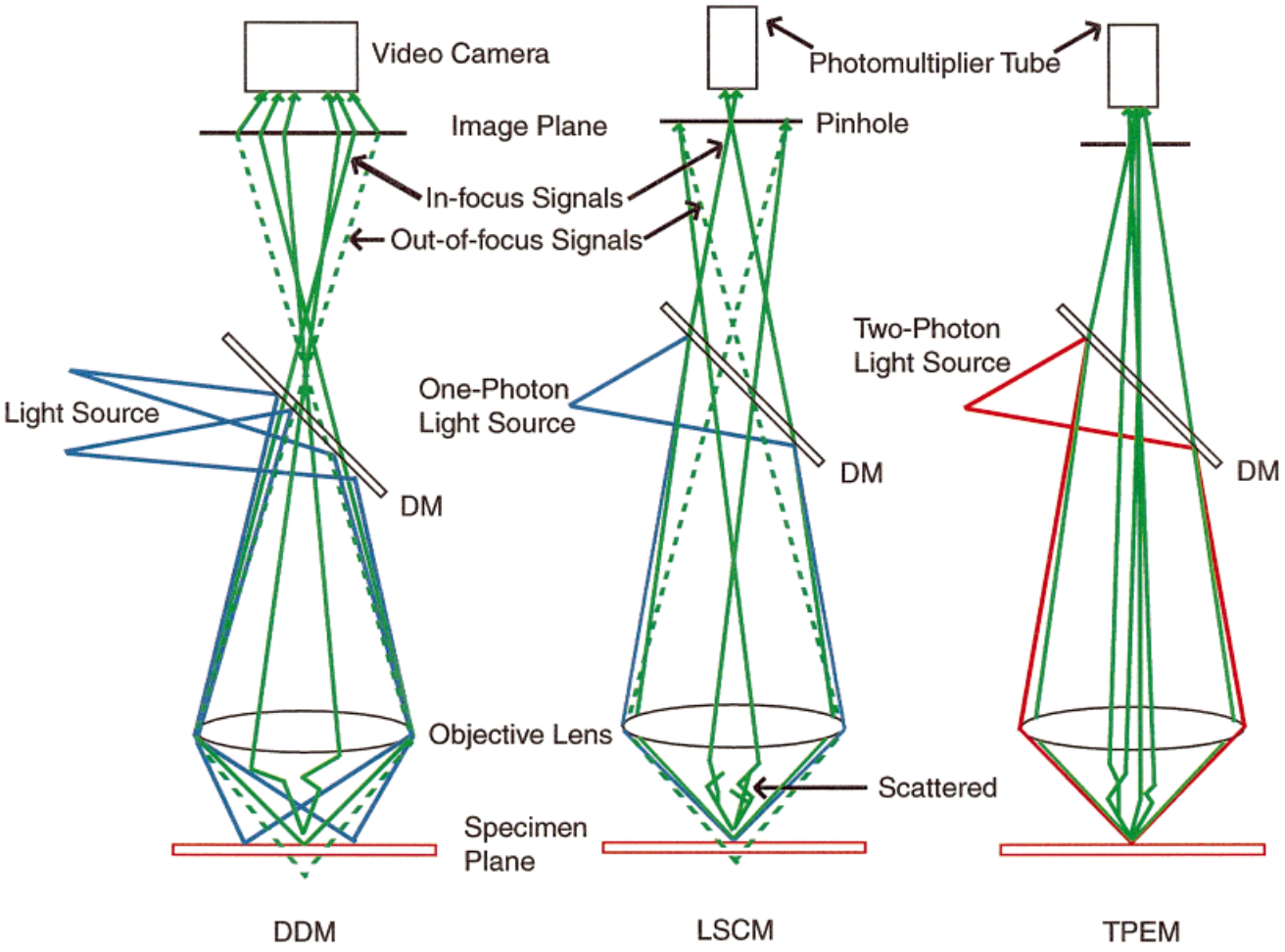

Fig. 3. Illustration of light illumination and detectors configuration used in one- and two-photon imaging systems. DM, dichroic mirror.

scattering, and achieves better depth discrimination for fluorescence imaging. The sensitivity of detection is much higher than for confocal microscopy because no aperture is required in the emission path and a greater number of photons reach the photodetector (see Fig. 3).

RESULTS AND DISCUSSION

The two-photon excitation (TPEM) approach has two significant advantages over the other tested methodologies: (1) it can see deeper and clearer into frog tissue than either deconvolution (DDM) or confocal microscopy (LSCM), and (2) it has the advantage of causing considerably less photodamage than the non-confocal excitation fluorescence techniques. To be a useful method for studying frog morphogenesis, several additional criteria must be met. First, the technique must be compatible with living frog tissue over a period of hours, at framing rates of 12–20/hour and with more z-series information collected. Second, imaging of the active cells must be possible in the tissues undergoing morphogenesis, and these can be buried in the tissue. For example, in the dorsal marginal zone, the cells that first undergo dramatic shape change are underneath a more static epithelium, at a depth of 20–30 μm. Therefore, any attempt to visualize these cells requires a technique that can resolve good images at a depth of more than 20 μm. Currently, the two-photon is the only tested fluorescence microscopy technique that meets these minimum requirements.

The TPEM image of cells under the epithelium was superior to conventional and confocal images of the same region of the specimen in terms of contrast and reduced "out-of-focus" information. The degree of improvement in image quality and depth penetration depends on the specimen, excitation power of the laser, laser pulse width, and the quality of imaging optics. We used the same objective lens for TPEM, LSCM, and DDM for better comparisons of signals. Nikon Plan Fluor objective lens provides better IR throughput than the Plan Apo lens.

To our knowledge, nothing is listed in the literature regarding the 2-photon absorption cross-section for Green Fluorescent Proteins. Watt Webb's group who invented the TPEM technology (Denk et al., 1990) has reported (unpublished data) that the peak excitation wavelength for EGFP is 970 nm. But we obtained maximum signal from the GFP-GAP-43 protein at 870 nm. The signal levels fall off on both side of the

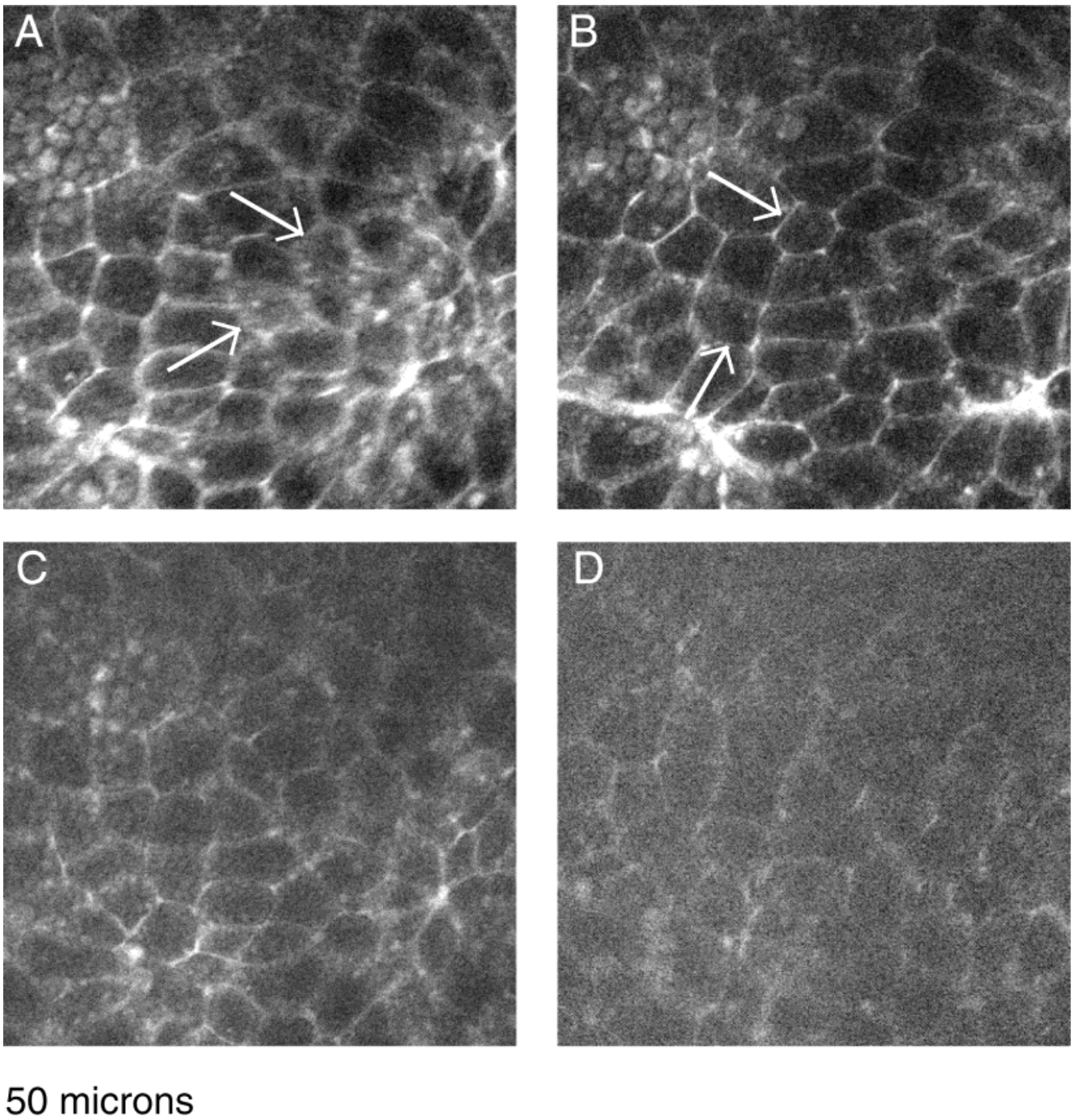

Fig. 4. Demonstration of excitation power versus signal-to-noise of two-photon images acquired at 870 nm at about 22 μm deep. The signal-to-noise of the image was better at 22-mW (**B**) compared to other average powers of excitation. (**A**) 25 mW; (**C**) 18 mW; (**D**) 11 mW.

spectrum. At the lower end of the spectrum, the background or autofluorescence from the tissue dominated the signal. It is also possible that the average power from the laser after 870 nm is not sufficient to generate more signal. Higher average power could be obtained by using a high pump power laser. In our current experimental setup, we have demonstrated that 870 nm and 22 mW average power are ideal for maximizing the signal-to-noise ratio.

In one-photon excitation, the fluorescence signal from the specimen could be improved by increasing the average power of the excitation laser. In two-photon excitation, the quality of the image did not improve just by increasing the average power of the excitation laser.

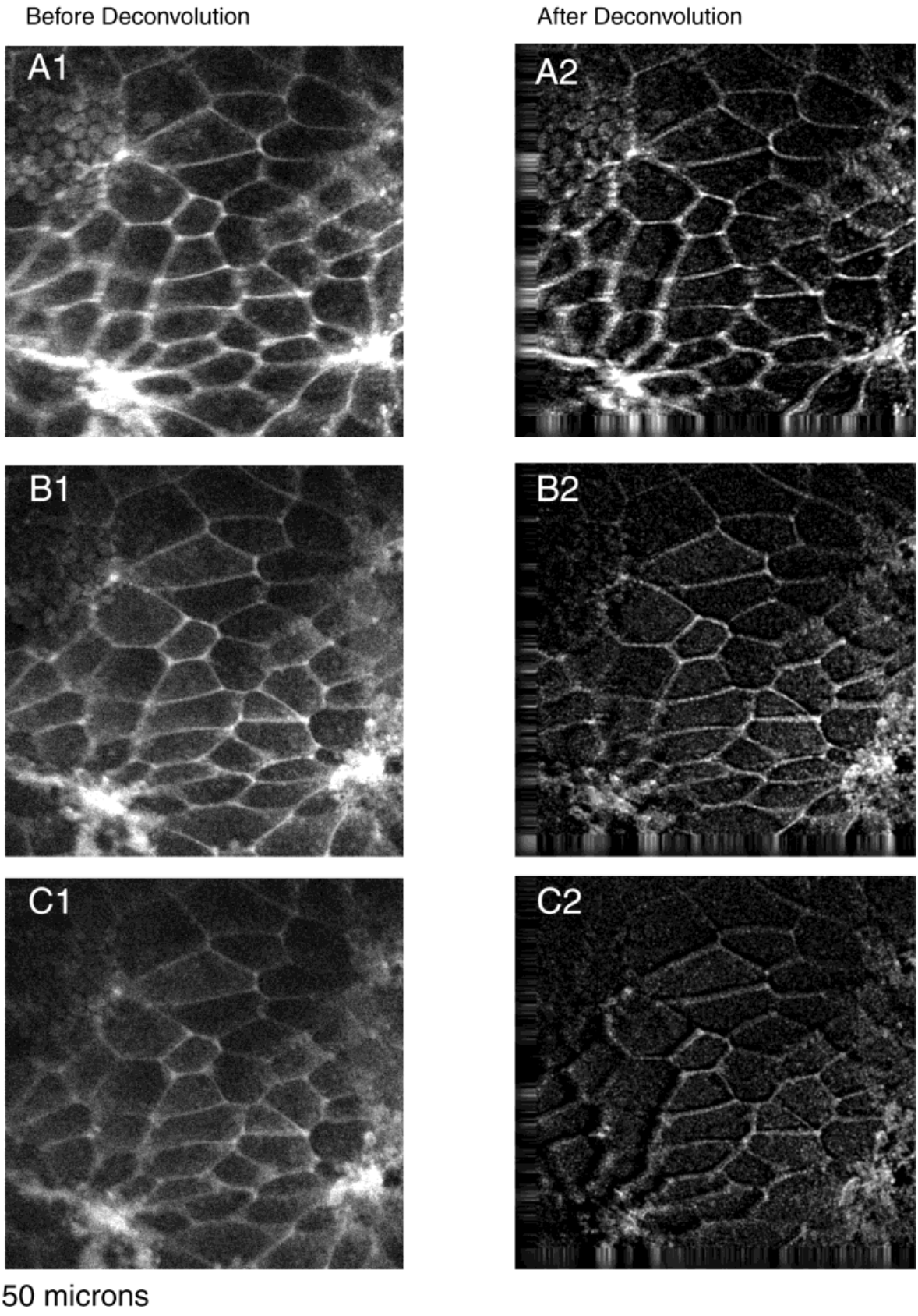

Fig. 5. The acquired two-photon images at different depths were deconvolved using Deltavision software. The deconvolution option helps to improve TPEM images by removing the background noise in deep tissue imaging. (**A**) 28 μm; (**B**) 34 μm; (**C**) 36 μm.

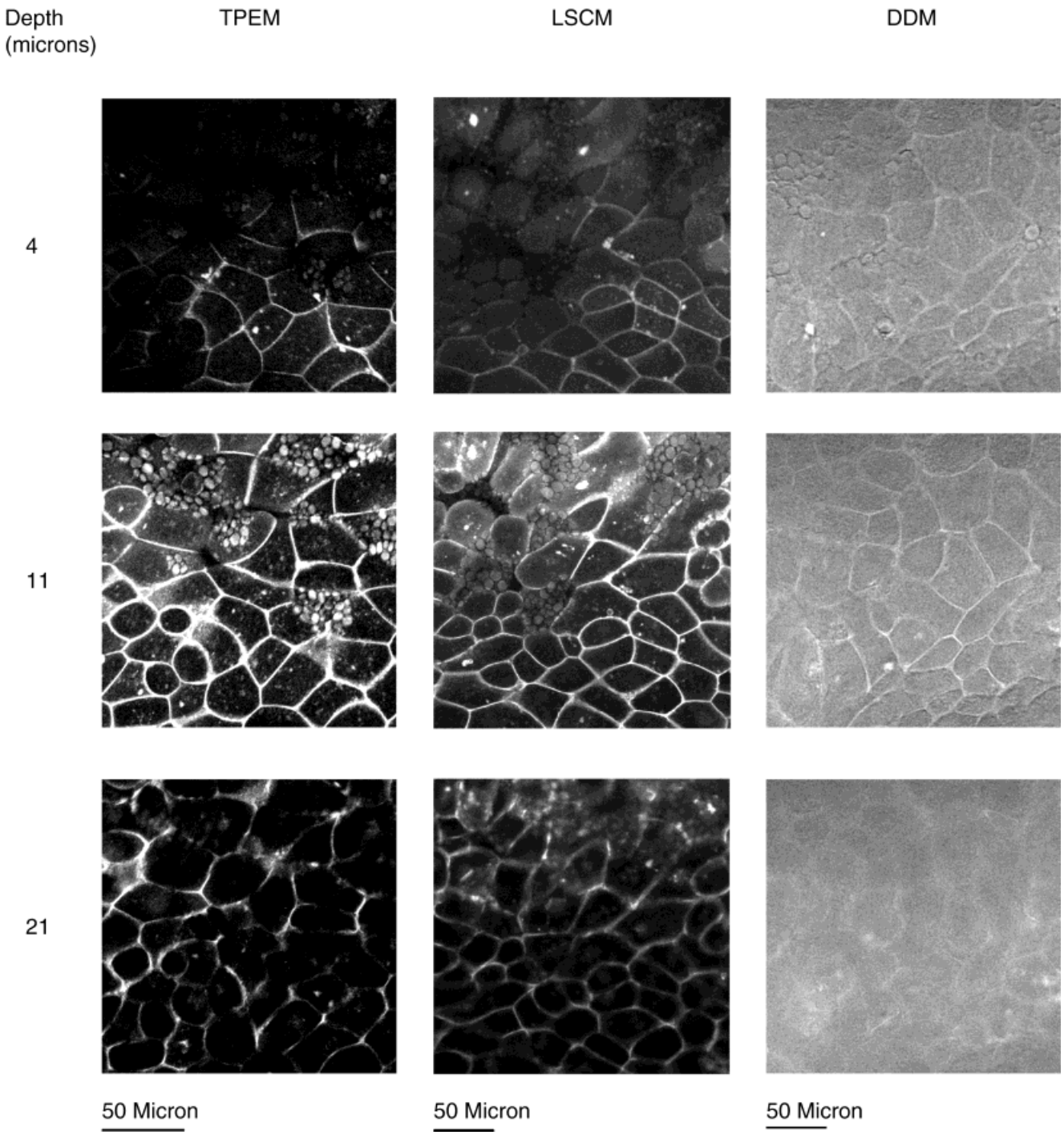

Fig. 6. Localization of GFP-GAP-43 fusion protein images in developing Xenopus embryos were acquired with same objective lens using Nikon epi-fluorescence based TPEM, LSCM, and DDM microscope system. The details of the images are superior in TPEM mode. Generally, deterioration and less details of information of GFP-GAP-43 proteins were observed in all sections of the tissue in LSCM mode. The DDM system is not good for tissue imaging as demonstrated in the figure (images were deconvolved (15 iterations) using Deltavision software).

To obtain better S/N in deep tissue, an optimum power level of excitation was required. As shown in Figure 4A, at 25 mW excitation power, the signal deteriorates relative to 22 mW (as indicated by arrows). The signal level or the image quality decreases with decreasing excitation power (see Fig. 4C,D). The cell images were sharp and clear at the power level 22 mW. This indicates that it is important to adjust the excitation power level depending on the specimen under investigation.

TABLE 1. Comparison of TPEM, LSCM and DDM imaging systems

	TPEM	LSCM	DDM
Light source	Infrared, picosecond or femtosecond pulsed lasers (tunable 700–1000 nm).	Visible/UV CW lasers (365, 488, 514, 543, 568, 633, 647 nm).	Visible/UV arc lamp any wavelength.
Illumination	Only at the focal point of the specimen.	Whole field of view.	Whole field of view.
Excitation/emission light	Wide separation (ex 730 nm; em 420 nm).	Close separation (ex 365 nm; em 420 nm).	Close separation (ex 365 nm; em 420 nm).
Detectors	Photomultiplier tube (PMT)—spot scanning. CCD Camera (Straub & Hell, 1998).	PMT, spot scanning CCD camera—Nipkow disk (Periasamy & Herman, 1994).	CCD camera whole field. High quantum efficiency compared to PMT.
Real-time imaging	Yes	Yes	No
Pinhole alignment	No	Yes	No
Photodamage and autofluorescence	Considerably less	High-compared to TPEM	High-compared to TPEM
Deep tissue imaging	Yes (>400 μm)	Yes, but considerably less than TPEM	Not good.
Signal-to-noise ratio	Enhanced	Ok	Ok
Resolution	Same as LSCM	Same as TPEM	Same but depending on algorithm used and the artifacts
Fluorophores	All common fluorophores	Selected fluorophores depending on the light source	All common fluorophores
Commercially available	Yes	Yes	Yes
Price	High	Less price compared to TPEM	Less price compared to TPEM & LSCM

The major advantage of the TPEM is its ability to image deep inside the tissue. It has been demonstrated that the TPEM can be used for >400 μm (Svoboda et al., 1997, 1999). Depending on the tissue sample, there is also a considerable amount of background signal dominating in the deep tissue imaging. We have demonstrated that the digital deconvolution software removes some of the background information in deep tissue imaging as shown in Figure 5. The deconvolution images improved the signal quality. Moreover, the deconvolution software would help to reveal various structural information hidden in biological specimens.

Figure 6 shows the comparison of TPEM, LSCM, and DDM at different depths. In our study, the deterioration of GFP-GAP-43 protein signal is clearly seen at 11 and 21μm deep in LSCM. In DDM, the localization of GFP-GAP-43 protein image was clear at 11 μm, but not at 21 μm. In all sections, two-photon signals are far superior to LSCM or DDM. Moreover, we did observe the photobleaching of the specimen, which was very low in the TPEM, compared with LSCM and DDM. The comparison of these three systems listed in Table 1 clearly demonstrates the advantages of TPEM over LSCM and DDM except the price. It is important to adjust the excitation intensity and the gain of the PMT to obtain better signal-to-noise (S/N) ratio in LSCM. DDM will be the ideal imaging system in cases where it is difficult to improve the S/N of the image. The DDM is not good for real-time calcium or deep tissue imaging, but is good for 3-dimensional double or triple labeling of cellular imaging. When compared with LSCM or DDM, the TPEM system is ideal for deep tissue imaging and for UV fluorophore excitation.

CONCLUSION

The TPEM system is a better system for deep tissue imaging provided that appropriate excitation wavelength, average power, and optics are chosen. The digital deconvolution software could help remove the background information obtained at deep tissue TPEM imaging. Most of our data acquisition was by descanning mode and more depth penetration could be improved by using an external PMT configuration in our present system. The ability to see >30 μm into frog gastrula tissue will allow high resolution time-lapse microscopy to reveal three-dimensional details about cells' interactions with each other as well as with extracellular matrix, during the morphogenesis of early development.

ACKNOWLEDGMENTS

We thank Bio-Rad, Coherent, C-Imaging, and Nikon for their valuable help and support to our imaging center.

REFERENCES

Agard DA, Hiraoka Y, Shaw P, Sedat JW. 1989. Fluorescence microscopy in three dimensions. Methods Cell Biol 30:353–377.

Bright GR, Taylor DL. 1986. Imaging at low light level in fluorescence microscopy. In: Taylor DL, Lanni F, Waggoner AS, Murphy RF, Birge RR, editors. Applications of fluorescence in the biomedical sciences. New York: Alan R. Liss. p 257–288.

Chalfie MTuY, Euskirchen G, Ward WW, Prasher DC. 1994. Green fluorescent protein as a marker for gene expression. Science 263:802–805.

Chen H, Swedlow JR, Grote M, Sedat JW, Agard DA. 1995. The collection, processing, and display of digital three-dimensional images of biological specimens. In: Pawley JM, editor. Handbook of biological confocal microscopy, 2nd ed. New York: Plenum Press. p 197–210.

Denk W, Strickler JH, Webb WW. 1990. Two-photon laser scanning fluorescence microscopy. Science 248:73–76.

Diaspro A, Beltrame F, Fato M, Ramoino P. 1996. Characterizing biostructure and cellular events in 2D/3D. IEEE Eng Med Biol 15:92–100.

Domingo C, Keller R. 1995. Induction of notochord cell intercalation behavior and differentiation by progressive signals in the gastrula of Xenopus laevis. Development 121:3311–3321.

Goppert-Mayer M. 1931. Ueber Elementarakte mit zwei Quantensprungen. Ann Phys 9:273–295.

Hell SW, Hanninen PE, Salo J, Kuusisto A, Soini E, Wilson T, Tan JB. 1994. Pulsed and CW confocal microscopy: A comparison of resolution and contrast. Optics Commun 113:144–152.

Hell SW, Bahlmann K, Schrader M, Soini A, Malak H, Gryczynski I, Lakowicz JR. 1996. Three-photon excitation in fluorescence microscopy. J Biomed Optic 1:71–74.

Inoué S, Spring K. 1997. Video microscopy. 2nd ed. New York: Plenum Press.
Keller R. 1991. Early embryonic development of *Xenopus laevis*. Methods Cell Biol 36:61–113.
Kim SH, Akihito Y, Bouwmeester T, Agius E, De Robertis EM. 1998. The role of Paraxial Protocadherin in selective adhesion and cell movements of the mesoderm during Xenopus gastrulation. Development 125:4681–4691.
Kintner C. 1988. Effects of altered expression of the neural cell adhesion molecule, N-CAM, on early neural development in Xenopus embryos. Neuron 1:545–555.
Kintner CR, Dodd J. 1991. Hensen's node induces neural tissue in Xenopus ectoderm. Implications for the action of the organizer in neural induction. Development 113:1495–1505.
Kintner CR, Melton DA. 1987. Expression of Xenopus N-CAM RNA in ectoderm is an early response to neural induction. Development 99:311–325.
Konig K, Liang H, Berns MW, Tromberg BJ. 1996. Cell damage in near-infrared multimode optical traps as a result of multiphoton absorption. Opt Lett 21:1090–1092.
Lakowicz JR. 1997. Topics in fluorescence microscopy. Nonlinear and two-photon-induced fluorescence, vol. 5. New York: Plenum Press.
Minsky M. 1957. U.S. Patent no. 3013467. Microscopy apparatus, Dec. 19, 1961 (Filed Nov. 7, 1957).
Nakamura O. 1992. Three-dimensional imaging characteristics of laser scan fluorescence microscopy: Two-photon excitation vs. single-photon excitation. Optik 93:39–42.
Nieuwkoop PD, Faber J. 1967. Normal table of *Xenopus laevis*. Amsterdam: North Holland.
Pawley J. 1995. Handbook of biological confocal microscopy, 2nd ed. New York: Plenum Press.
Periasamy A. 1998. Digital deconvolution FRET microscopy: 3D visualization of protein-protein interactions in a single living cell. SPIE 3260:106–114.
Periasamy A. 1999. Multi-photon excitation fluorescence imaging microscopy in the biomedical sciences. SPIE 3604:74–82.
Periasamy A, Herman B. 1994. Computerized fluorescence microscopic vision in the biomedical sciences. J Comput Assist Microsc 6:1–26.
Piston DW, Kirby MS, Cheng H, Lederer WJ, Webb WW. 1994. Two photon-excitation fluorescence imaging of three-dimensional calcium-ion-activity. Appl Optics 33:662–669.
Potter SM. 1996. Vital imaging: two photons are better than one. Curr Biol 6:1595–1598.
Potter SM, Wang C, Garrity PA, Fraser SE. 1996. Intravital imaging of green fluorescent protein using two-photon laser scanning microscopy. Gene 173:25–31.
Shaw PJ. 1993. Computer reconstruction in three-dimensional fluorescence microscopy. In: Shotton, D., editor. Electronic light microscopy. New York: Wiley-Liss. P 211-230.
Shih J, Keller R. 1992a. Cell motility driving mediolateral intercalation in explants of Xenopus laevis. Development 116:901–914.
Shih J, Keller R. 1992b. Patterns of cell motility in the organizer and dorsal mesoderm of Xenopus laevis. Development 116:915–930.
Shotton DM. 1989. Confocal scanning optical microscopy and its applications for biological specimens. J Cell Sci 94:175–206.
So PTC, French T, Yu WM, Berland KM, Dong CY, Gratton E. 1995. Time-resolved fluorescence microscopy using two-photon excitation. Bioimaging 3:49–63.
Spemann H. 1938. Embryonic development and induction. New Haven: Yale University Press.
Straub M, Hell SW. 1998. Multifocal multiphoton microscopy: A fast and efficient tool for 3-D fluorescence imaging. Bioimaging 6:177–185.
Sullivan KF, Kay SA. 1999. Green fluorescent proteins. Methods Cell Biol, Vol. 58. New York: Academic Press.
Svoboda K, Denk W, Kleinfeld, D, Tank, DW. 1997. In vivo dendriti calcium dynamics in neocortical pyramidal neurons. Nature 385:161–165.
Svoboda K, Helmchen F, Denk W, Tank, DW. 1999. Spread of dendritic excitation in layer 2/3 pyramidal neurons in rat barrel cortex in vivo. Nat Neurosci 2:65–73.
Tsien RY. 1989. Fluorescent indicators of ion concentrations. Methods Cell Biol 30:127–156.
Van der Voort HTM, Brakenhoff GJ. 1988. Determination of the 3-dimensional optical properties of a confocal scanning laser microscope. Optik 78:48–53.
White JG, Amos, WB, Fordham M. 1987. An evaluation of confocal versus conventional imaging of biological structures by fluorescence light microscopy. J Cell Biol 105:41–48.
Wilson T, Sheppard JR. 1984. Theory and practice of scanning optical microscopy. New York: Academic Press.
Wokosin DL, Centonze V, White JG, Armstrong D, Robertson G, Ferguson AI. 1996. All-solid-state ultrafast lasers facilitate multiphoton excitation fluorescence imaging. IEEE J Select Topics Quantum Electron 2:1051–1065.